Origin of the large positive magnetoresistance of $Ge_{1-x}Mn_x$ granular thin films

Yuki K. Wakabayashi,[1,*] Ryota Akiyama,[2] Yukiharu Takeda,[3] Masafumi Horio,[2] Goro Shibata,[2] Shoya Sakamoto,[2] Yoshisuke Ban,[1] Yuji Saitoh,[3] Hiroshi Yamagami,[3,4] Atsushi Fujimori,[2] Masaaki Tanaka,[1,5] and Shinobu Ohya[1,5,†]

[1]*Department of Electrical Engineering and Information Systems, The University of Tokyo, 7-3-1 Hongo, Bunkyo-ku, Tokyo 113-8656, Japan*

[2]*Department of Physics, The University of Tokyo, Bunkyo-ku, Tokyo 113-0033, Japan*

[3]*Materials Sciences Research Center, Japan Atomic Energy Agency (JAEA), Sayo, Hyogo 679-5148, Japan*

[4]*Department of Physics, Kyoto Sangyo University, Motoyama, Kamigamo, Kita-Ku, Kyoto 603-8555, Japan*

[5]*Center for Spintronics Research Network, Graduate School of Engineering, The University of Tokyo, 7-3-1 Hongo, Bunkyo-ku, Tokyo 113-8656, Japan*

(Received 14 June 2016; revised manuscript received 16 November 2016; published 17 January 2017)

$Ge_{1-x}Mn_x$ (GeMn) granular thin films are a unique and promising material for spintronic applications owing to their large positive magnetoresistance (MR). Previous studies of GeMn have suggested that the large MR is related to the nanospinodal decomposition of GeMn into Mn-rich ferromagnetic nanoparticles and a Mn-poor paramagnetic matrix. However, the microscopic origin of the MR has not yet been clarified. Here, we develop a method to separately investigate the magnetic properties of the nanoparticles and the matrix, utilizing the extremely high sensitivity of x-ray magnetic circular dichroism (XMCD) to the local magnetic state of each atom. We find that the MR ratio is proportional to the product of the magnetizations originating from the nanoparticles and the matrix. This result indicates that the spin-polarized holes in the nanoparticles penetrate into the matrix and that these holes undergo first order magnetic scattering by the paramagnetic Mn atoms in the matrix, which induces the large MR.

DOI: 10.1103/PhysRevB.95.014417

I. INTRODUCTION

$Ge_{1-x}Mn_x$ (GeMn) granular thin films have attracted much interest for spintronic applications owing to their large positive magnetoresistance (MR), which can be as high as ∼280% (under 5 T at 40 K), and their compatibility with existing semiconductor technology [1–9]. In GeMn, the sharp enhancement of the MR at very low temperatures and its peculiar spike-shaped magnetic field dependence cannot be explained by conventional effects, such as giant magnetoresistance (GMR) [10] and magnetic field-dependent avalanche breakdown [11,12], which are widely invoked to explain the origin of the MR of granular films. Previous studies of GeMn have suggested that the large MR is related to nanoscale spinodal decomposition of GeMn into ferromagnetic (FM) metallic Mn-rich nanoparticles and a paramagnetic (PM) Mn-poor matrix (Fig. 1) [2,3,7,8]. However, the microscopic origin of the MR has not yet been clarified over the past decade since the first report of GeMn, although understanding the microscopic origin of the MR is vitally important for the development of spin-dependent functionality in granular films. Generally, the origin of the MR in granular systems is discussed in the context of the *macroscopic* properties of the transport and magnetization of the films. For a more profound understanding of the MR, however, it is obvious that we need *microscopic* information. Because the large MR of GeMn is thought to be induced by spin-dependent scattering near the interfaces between the nanoparticles and the matrix, separate detection of the magnetic properties of the FM nanoparticles and the PM matrix near the interfaces is necessary. However, this is difficult with conventional magnetization measurements using a superconducting quantum interference device (SQUID).

Soft x-ray magnetic circular dichroism (XMCD) is extremely sensitive to the local magnetic state of each atom in magnetic films [13–18]. One can distinguish between the different local magnetic states based on the difference in the energy spectrum in addition to the difference in the magnetic-field dependence of the XMCD signal from each atom. Thus, by carefully analyzing the magnetic-field dependence of the XMCD signals using various incident photon energies, it would be possible to distinguish the magnetic signals originating from the FM nanoparticles from those originating from the PM matrix. Another advantage of XMCD, especially in our paper, is its probing depth. In the total electron yield (TEY) mode used for the present XMCD measurements, we detect signals originating from atoms located within 2–3 nm of the film surface [19]. As shown in Fig. 1, the nanoparticles are located approximately 3–5 nm from the film surface of GeMn. Thus, one can selectively study the magnetic properties near the top interfaces of those nanoparticles. Because the scattering of charge carriers occurs near those interfaces, XMCD measurements are suitable for the investigation of first order magnetic scattering in GeMn. In addition, because XMCD is free from the diamagnetic signal from the substrate, one can perform very accurate measurements. Despite these attractive features, there have been no reports of selective detection of the magnetizations of the nanoparticles and matrix in magnetic granular films using XMCD.

In this paper, we demonstrate a method to separately investigate the magnetic properties of the nanoparticles and the matrix in GeMn granular thin films. We clarify the origin of the large MR, the peculiar magnetic field dependence, and the large enhancement at low temperatures. We make full use of the aforementioned advantages of XMCD and carefully analyze the XMCD data. We find that the MR

*Corresponding author: wakabayashi@cryst.t.u-tokyo.ac.jp
†Corresponding author: ohya@cryst.t.u-tokyo.ac.jp

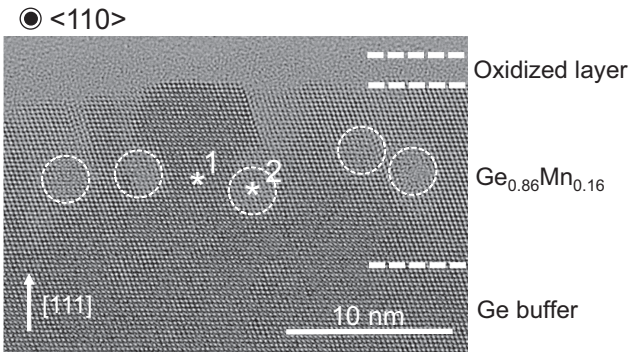

FIG. 1. Transmission electron microscope lattice image of the $Ge_{0.86}Mn_{0.14}$ layer projected along the Ge⟨110⟩ axis. The nanoparticles are indicated by white dashed circles. By the spatially resolved energy dispersive x-ray spectroscopy, the local Mn concentrations at *1 (matrix) and *2 (nanoparticle) are estimated to be ∼6 and ∼60%, respectively.

ratio is proportional to the product of the magnetizations originating from the FM nanoparticles and the PM matrix. This indicates that the spin-polarized holes, which penetrate from the nanoparticles into the matrix, undergo first order magnetic scattering by the PM Mn atoms in the matrix, thereby causing the large MR.

II. SAMPLE STRUCTURES AND CRYSTALLOGRAHIC ANALYSES

We grew 13-nm-thick epitaxial $Ge_{1-x}Mn_x$ granular thin films with average Mn concentrations x of 0.09 and 0.14 on p- (or n-) type Ge(111) substrates using low-temperature molecular beam epitaxy (see Sec. I of the Supplemental Material [20]). To avoid parallel conduction through the substrate, the samples for the magnetotransport measurements were grown on n-type substrates because GeMn is p-type, and the $p-n$ junction of p-GeMn/n-Ge prevents carrier diffusion from the GeMn layer to the substrate [21]. For other samples, after the growth of the $Ge_{1-x}Mn_x$ layer, we grew a 1.5-nm-thick Ge capping layer to prevent surface oxidation of the $Ge_{1-x}Mn_x$ layer. Our transmission electron microscope analyses indicated that the GeMn films have spherelike Mn-rich nanoparticles and a Mn-poor surrounding matrix (Fig. 1). The nanoparticles are located 3–5 nm from the film surface. They have an amorphous metallic GeMn phase, including Mn_5Ge_3 precipitates [3,8,22]. The Mn-poor surrounding matrix has a diamond-type crystal structure (see Sec. II of the Supplemental Material [20]). Using spatially resolved energy dispersive x-ray spectroscopy, the local Mn concentration in the nanoparticles of the $Ge_{0.86}Mn_{0.14}$ film was estimated to be ∼60%, whereas that in the matrix of the $Ge_{0.86}Mn_{0.14}$ film was estimated to be ∼6%. Because we obtained similar XMCD results both for the $Ge_{0.91}Mn_{0.09}$ and $Ge_{0.86}Mn_{0.14}$ samples, as shown later (Fig. 4), we can estimate that the ratio of the local Mn concentration of the Mn-rich nanoparticles to that of the Mn-poor-matrix is roughly similar between the two samples. Then, the local Mn concentrations in the nanoparticles and the matrix in the $Ge_{0.91}Mn_{0.09}$ film are estimated to be ∼40 and ∼4%,

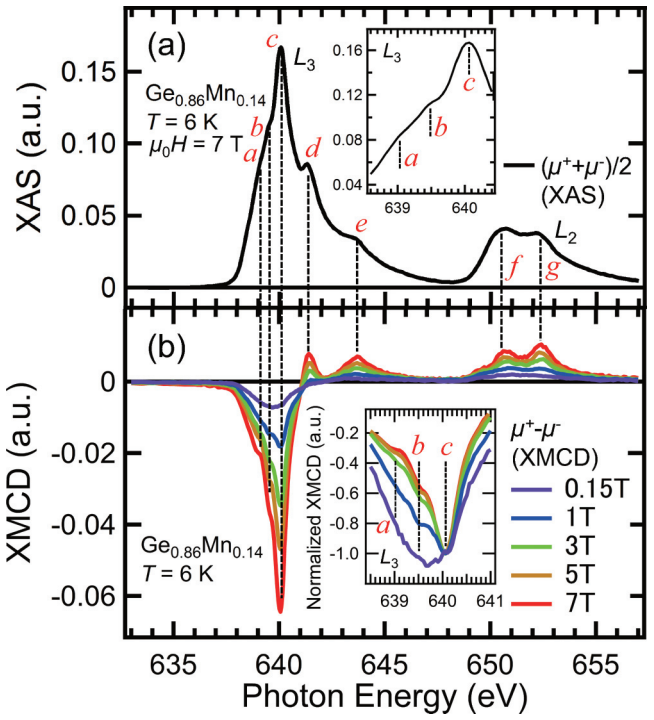

FIG. 2. (a) Mn $-$ $L_{2,3}$ edge XAS $[(\mu^+ + \mu^-)/2]$ spectrum for the $Ge_{0.86}Mn_{0.14}$ film at 6 K with a magnetic field $\mu_0 H = 7$ T applied perpendicular to the film surface. The inset shows a magnified plot of the spectrum at the Mn $-$ L_3 edge. (b) Mn $-$ $L_{2,3}$ edge XMCD $(= \mu^+ - \mu^-)$ spectra for the $Ge_{0.86}Mn_{0.14}$ film at 6 K with various magnetic fields H applied perpendicular to the film surface. The inset shows a magnified plot of the spectra at the Mn $-$ L_3 edge. Here, the XMCD data have been normalized at c.

respectively. Most of the 1.5-nm-thick Ge capping layer is naturally oxidized in the atmosphere. To remove this layer, the samples were briefly etched in dilute HF solution prior to loading them into the XMCD vacuum chamber. Before performing the measurements, we carefully checked and confirmed the *absence* of a two-peak structure at 537 and 540 eV, which originates from the Mn oxide on the sample surface, using x-ray absorption spectroscopy (XAS) [23].

III. THE XAS AND XMCD MEASUREMENTS

For the XAS and XMCD measurements, we used the twin-helical undulator beamline BL23SU of SPring-8, which enabled us to perform efficient measurements of XMCD with various incident photon energies and magnetic fields at various temperatures [24]. Figure 2 shows the Mn $-$ $L_{2,3}$ edge XAS $[(\mu^+ + \mu^-)/2]$ spectrum (a) and the XMCD $(= \mu^+ - \mu^-)$ spectra (b) for the $Ge_{0.86}Mn_{0.14}$ film at 6 K, with various magnetic fields applied perpendicular to the film surface. The direction of the incident x-ray is also perpendicular to the film surface. Here, μ^+ and μ^- refer to the absorption coefficients for the photon helicity parallel and antiparallel to the Mn 3d majority spin direction, respectively. In both the XAS and XMCD spectra, one can see five peaks at the Mn $-$ L_3 edge (whose energies are referred to as $a-e$) [see also the insets in Figs. 2(a) and 2(b)] and two peaks at the Mn $-$ L_2 edge (whose energies are referred to as f and g). When the XMCD

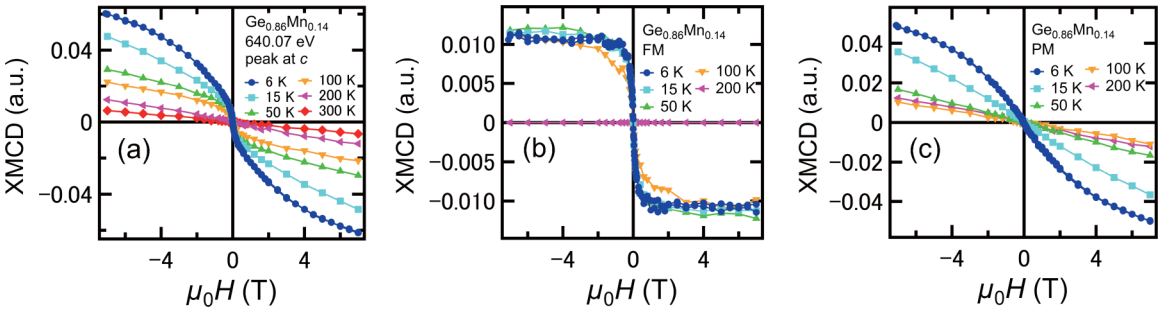

FIG. 3. (a)–(c) Experimentally obtained XMCD-H curves (a) and derived FM (b) and PM (c) components of the XMCD-H curves for the $Ge_{0.86}Mn_{0.14}$ film at various temperatures.

spectra are normalized at c, the spectral line shape is changed with varying H, and the peak at c becomes more dominant as H increases, as shown in the inset of Fig. 2(b). Whereas the XMCD intensities at a and b tend to saturate for $\mu_0 H = 7$ T, the one at c does not. This indicates that the peaks at a and b have a certain amount of an FM component, whereas the peak at c mainly originates from the PM Mn atoms. The same features were also observed in the $Ge_{0.91}Mn_{0.09}$ film (see Fig. S3 in Sec. III of the Supplemental Material [20]). These results indicate that the XMCD signals have both PM and FM components.

By analyzing the XMCD-H curves measured at various energies and temperatures T for both samples with $x = 0.09$ and 0.14, we decomposed the XMCD signals into an FM (-like) component, which saturates at high magnetic fields (>6 T), and a PM component, which is linear in the range of $\mu_0 H$ from −1 to 1 T and follows the Brillouin function (for the detailed procedure, see Secs. IV and V of the Supplemental Material [20]). One example of the decomposition of the XMCD signal for $Ge_{0.86}Mn_{0.14}$ is shown in Fig. 3. At all temperatures, we succeeded in decomposing the XMCD-H curves into FM and PM components. Furthermore, all the XMCD-H curves measured with different energies are expressed by linear combinations of the FM and PM XMCD-H curves shown in Figs. 3(b) and 3(c) (see Fig. S5 in Sec. IV of the Supplemental Material [20]). This means that there exist only two components (FM and PM components) in the XMCD signals. The following results verify our decomposition procedure of the XMCD signals. The Curie plot (H/XMCD − T) of the derived PM component of the XMCD was linear, which is typical PM behavior and confirms that the PM component is derived correctly in our paper (see Fig. S9 in Sec. VI of the Supplemental Material [20]). In Fig. 3(b), the FM component of the XMCD becomes zero at 200 K, which means that local ferromagnetism appears below 200 K [2,3,7,8]. This result is consistent with previous studies of GeMn granular films [2,3,7,8]. Similar features were also observed in $Ge_{0.91}Mn_{0.09}$ (see Fig. S8 in Sec. V of the Supplemental Material [20]).

From the above analysis, we derived the FM and PM components of the XMCD signal at various energies for both samples, as shown by the green and blue points in Fig. 4, respectively, for both samples. The FM component of the XMCD spectra has a broad single negative peak at the Mn − L_3 edge. This is a typical feature that can be observed for the delocalized 3d electrons of the FM Mn atoms in metallic materials. This result confirms that the FM component indeed originates from the Mn-rich nanoparticles, each of which is locally metallic. The PM component of the XMCD signal is attributed to the Mn-poor matrix. The derived XAS spectra of the PM Mn atoms have three peaks at the Mn − L_3 edge (see Sec. VII of the Supplemental Material [20]), which is consistent with the result of the first-principles calculation of the XAS spectrum of the Mn atoms that substitute for Ge atoms in $Ge_{1-x}Mn_x$ [25]. The PM component of the XMCD spectra has three peaks at

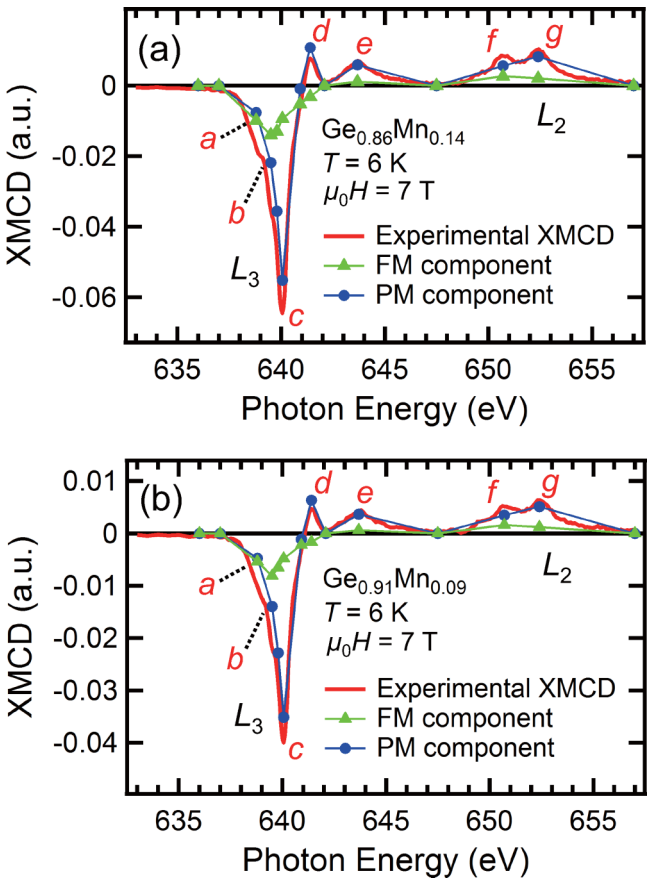

FIG. 4. (a) and (b) Experimentally obtained XMCD spectra (red curve), derived FM (green triangles), and PM (blue circles) components of the XMCD spectra at 6 K with $\mu_0 H = 7$ T applied perpendicular to the film surface for the $Ge_{0.86}Mn_{0.14}$ film (a) and $Ge_{0.91}Mn_{0.09}$ film (b).

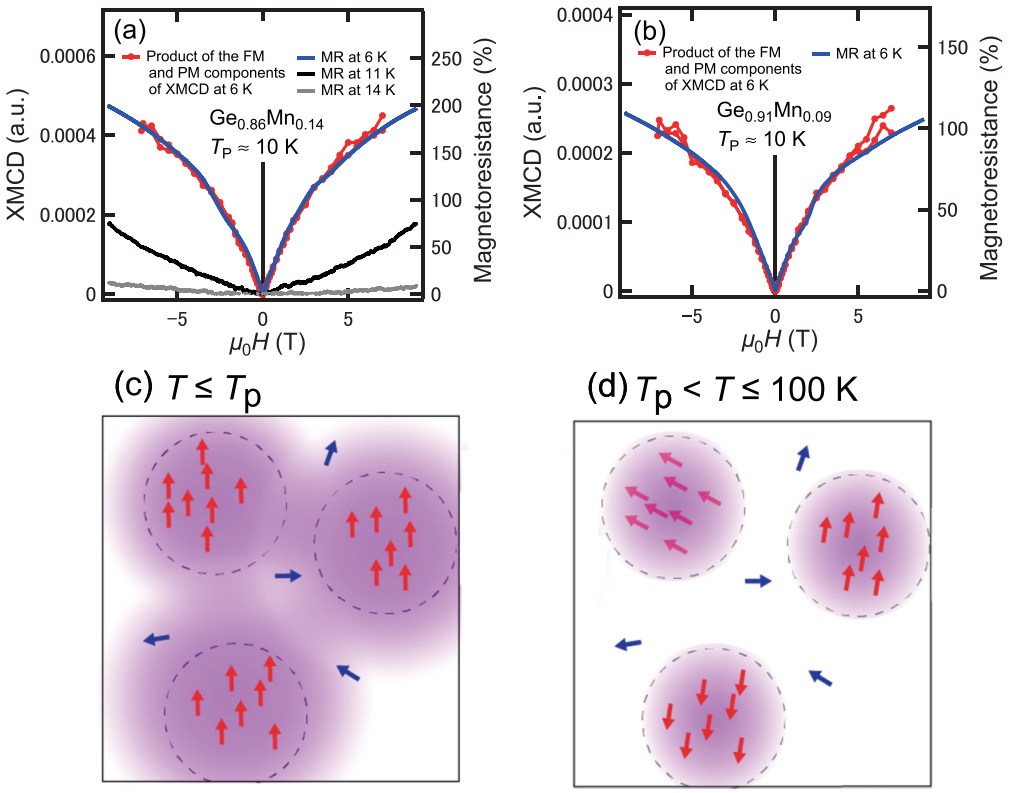

FIG. 5. (a) and (b) MR ratio (blue, black, and gray curves) as a function of $\mu_0 H$ applied perpendicular to the film surface for the $Ge_{0.86}Mn_{0.14}$ film (a) and the $Ge_{0.91}Mn_{0.09}$ film (b). The magnetic field dependence of the product of the FM and PM components of the XMCD intensity is also plotted (red points and curves). (c) and (d) Schematic illustration of the spatial distribution of the spin-polarized holes (pink regions) originating from the Mn-rich nanoparticles (black dashed circles) when the temperature $T \leqslant T_p$ (c) and $T_p < T \leqslant 100$ K (d). The red and blue arrows correspond to the magnetic moments of the Mn atoms in the FM nanoparticles and PM matrix, respectively.

c, d, and e and shows the sign change at 641 eV at the Mn $- L_3$ edge (Fig. 4). These are the characteristic features of the localized $3d$ state of the Mn^{2+} ions with a magnetic moment of $5\,\mu_B$ [17,26,27]. From the Brillouin function that expresses the PM component of the XMCD-H curve at 6 K, the magnetic moment of the PM component is also estimated to be $5\,\mu_B$ (see Figs. S4(d) and S6(d) in Sec. IV of the Supplemental Material [20]). This magnetic moment is clearly different from a theoretically predicted value ($3\,\mu_B$) for FM Mn atoms that substitute for Ge atoms [28], which supports our understanding that this component originates from the PM Mn atoms. These are characteristic features of the Mn atoms in insulating materials and are consistent with the insulating behavior of the matrix region of GeMn, which is evidenced by the variable range hopping transport observed in GeMn [3,8]. Additionally, the estimated spin and orbital magnetic moments of the Mn-rich nanoparticles and the Mn-poor matrix support the abovementioned assignment of the FM and PM components to the nanoparticles and matrix, respectively (see Sec. VIII of the Supplemental Material [20]).

Because XMCD preferentially detects Mn atoms located near the top interfaces of the nanoparticles, the magnetic properties obtained via SQUID, which detects the magnetic properties of the entire film, are different from our XMCD results. Whereas we do not see hysteresis in the XMCD-H curves (Fig. 3), it is observed in the SQUID measurements (see Fig. S14 in Sec. IX of the Supplemental Material [20]) [8,29]. Thus, in the nanoparticles, the magnetic property of the interface is different from that at the core. As mentioned below, the holes located near these interfaces experience first order magnetic scattering and thus have a key role in causing the large MR. This means that the selective detection capability of XMCD is uniquely suited for investigation of first order magnetic scattering in GeMn.

IV. MAGNETOTRANSPORT MEASUREMENTS

The blue, black, and gray curves in Figs. 5(a) and 5(b) show the MR ratio, defined as $[\rho(H) - \rho(0)]/\rho(0)$, of the $Ge_{0.86}Mn_{0.14}$ (a) and $Ge_{0.91}Mn_{0.09}$ (b) films. Here, $\rho(H)$ represents the resistivity of the GeMn films with H applied perpendicular to the film surface. The magnetic field dependence of the product of the FM and PM components of the XMCD intensity is also plotted (red curves). Below the percolation temperature ($T_p \approx 10$ K) of GeMn [8,30], the MR curves for both samples exhibit a spike-shaped curve, which is specific to the GeMn granular films. Additionally, the MR exhibits a large enhancement below T_p. The MR ratio reaches 199 and 109% at 6 K ($<T_p$) when $\mu_0 H = 9$ T in $Ge_{0.86}Mn_{0.14}$ and $Ge_{0.91}Mn_{0.09}$, respectively. We see that the MR ratio is proportional to the product of the FM and PM components of the XMCD intensities [Figs. 5(a) and 5(b)]. This means that the MR is induced by first order magnetic scattering of

spin-polarized holes [31], which is expressed as

$$\mathrm{MR} = -4P_{\mathrm{FM}}\frac{M_{\mathrm{FM}}(H)}{|M_{\mathrm{FM}}(H)|}\frac{J_{pd}}{g\mu_{\mathrm{B}}V}M_{\mathrm{PM}}(H), \quad (1)$$

where P_{FM}, J_{pd}, g, V, $M_{\mathrm{FM}}(H)$, and $M_{\mathrm{PM}}(H)$ represent the spin polarization of holes in the FM regions, the *p-d* exchange coupling constant between the holes and the PM Mn atoms, the g factor, the field-independent part of the potential, the magnetization of the FM Mn atoms, and the magnetization of the PM Mn atoms, respectively. The sign of the MR depends on the signs of P_{FM} and J_{pd}. Because the sign of the observed MR in our GeMn film is different from that of InMnSb [31], the sign of either P_{FM} or J_{pd} of GeMn should be different from that of InMnSb. Generally, below T_{p}, spin-polarized holes in the FM Mn-rich regions penetrate into the Mn-poor matrix and overlap with other holes that are extended from different Mn-rich nanoparticles [see Figs. 5(c) and 5(d)]. This induces percolation and long-range FM ordering [2,3,7,8,30]. Thus, our results indicate that the spin-polarized holes, which are extended from the nanoparticles, undergo first order magnetic scattering from the PM Mn atoms in the matrix below T_{p} and that this scattering induces the large positive MR [2,3,7,8].

When $T > T_{\mathrm{p}}$, the MR was significantly reduced, and the shape of the MR curve changed to concave [Fig. 5(a)], which means that the origin of the MR is different between $T > T_{\mathrm{p}}$ and $T < T_{\mathrm{p}}$. The MR above T_{p} does not follow a parabolic curve, which indicates that it is not a conventional MR that originates from the Lorentz force. In GeMn, the resistivity has a bump at $T = T_{\mathrm{p}}$ [3,8]. By increasing H, the spins tend to be aligned, and percolation can occur more easily, which leads to an increase in T_{p}. Thus, when $T > T_{\mathrm{p}}$, the resistivity increases with increasing H, reflecting the approach of T_{p} to the measurement temperature [2,3,8]. This induces the small positive MR when $T > T_{\mathrm{p}}$.

If we take $|\frac{J_{pd}}{V}| = 0.17$, as reported in (In,Mn)Sb [31], the absolute value of the spin polarization of the holes in the FM nanoparticles is estimated to be 64%. This large spin polarization is thought to be the origin of the large MR in GeMn below T_{p}, making GeMn a promising material for future spintronic applications. Via careful analysis of the XMCD results, we separately obtained the detailed magnetic properties of the Mn-rich nanoparticles and the Mn-poor matrix. This method will also be useful for other granular materials and magnetic multilayers and will help to understand the mechanism of the MR and yield insight into how to increase the MR ratios of these systems.

V. SUMMARY

In summary, we developed a method to investigate the magnetic properties of the FM nanoparticles and the PM matrix in GeMn granular thin films separately by utilizing the extremely high sensitivity of XMCD to the local magnetic state of each atom. We revealed that the MR ratio is proportional to the product of the magnetizations of the FM nanoparticles and the PM matrix when $T < T_{\mathrm{p}}$. Below T_{p}, the spin-polarized holes in the FM nanoparticles penetrate into the Mn-poor matrix. Thus, the large MR can be associated with first order magnetic scattering of these extended spin-polarized holes by the PM Mn atoms in the Mn-poor matrix. The absolute value of the spin polarization of the holes in the FM nanoparticles is estimated to be 64%. The large spin polarization makes $Ge_{1-x}Mn_x$ a promising material for future spintronic applications.

ACKNOWLEDGMENTS

This paper was partly supported by Grants-in-Aid for Scientific Research (Grants No. 22224005, No. 23000010, No. 26249039, and No. 15H02109), including the Specially Promoted Research program, the Project for Developing Innovation Systems from Ministry of Education, Culture, Sports, Science and Technology (MEXT), the Cooperative Research Project Program of Research Institute of Electrical Communication (RIEC), Tohoku University, and the Spintronics Research Network of Japan. This work was performed under the Shared Use Program of Japan Atomic Energy Agency (JAEA) Facilities (Proposal No. 2015B-E24) with the approval of the Nanotechnology Platform Project supported by MEXT. The synchrotron radiation experiments were performed at the JAEA beamline BL23SU in SPring-8 (Proposal No. 2015B3881). Y.K.W. acknowledges financial support from Japan Society for the Promotion of Science (JSPS) through the Program for Leading Graduate Schools (MERIT) and the JSPS Research Fellowship Program for Young Scientists. S.S. acknowledges financial support from JSPS through the Program for Leading Graduate Schools (ALPS).

[1] Y. D. Park, A. T. Hanbicki, S. C. Erwin, C. S. Hellberg, J. M. Sullivan, J. E. Mattson, T. F. Ambrose, A. Wilson, G. Spanos, and B. T. Jonker, Science **295**, 651 (2002).

[2] A. P. Li, J. Shen, J. R. Thompson, and H. H. Weitering, Appl. Phys. Lett. **86**, 152507 (2005).

[3] A. P. Li, J. F. Wendelken, J. Shen, L. C. Feldman, J. R. Thompson, and H. H. Weitering, Phys. Rev. B **72**, 195205 (2005).

[4] M. Jamet, A. Barski, T. Devillers, V. Poydenot, R. Dujardin, B.-G. Pascale, J. Rothman, B.-A. Edith, A. Marty, J. Cibert, R. Mattana, and S. Tatarenko, Nat. Mater. **5**, 653 (2006).

[5] I.-S. Yu, M. Jamet, T. Devillers, A. Barski, P. Bayle-Guillemaud, C. Beigne, J. Rothman, V. Baltz, and J. Cibert, Phys. Rev. B **82**, 035308 (2010).

[6] P. Dalmas de Reotier, E. Prestat, P. Bayle-Guillemaud, M. Boukhari, A. Barski, A. Marty, M. Jamet, A. Suter, T. Prokscha, Z. Salman, E. Morenzoni, and A. Yaouanc, Phys. Rev. B **91**, 245408 (2015).

[7] R. B. Morgunov, A. I. Dmitriev, and O. L. Kazakova, Phys. Rev. B **80**, 085205 (2009).

[8] R. Akiyama, R. Nakane, Y. K. Wakabayashi, and M. Tanaka (unpublished)

[9] C. Jaeger, C. Bihler, T. Vallaitis, S. T. B. Goennenwein, M. Opel, R. Gross, and M. S. Brandt, Phys. Rev. B **74**, 045330 (2006).
[10] J.-Q. Wang and G. Xiao, Phys. Rev. B **49**, 3982 (1994).
[11] H. Akinaga, M. Mizuguchu, K. Ono, and M. Oshima, Appl. Phys. Lett. **76**, 357 (2000).
[12] M. Yokoyama, T. Ogawa, A. M. Nazmul, and M. Tanaka, J. Appl. Phys. **99**, 08D502 (2006).
[13] S. Ahlers, P. R. Stone, N. Sircar, E. Arenholz, O. D. Dubon, and D. Bougeard, Appl. Phys. Lett. **95**, 151911 (2009).
[14] D. J. Keavney, D. Wu, J. W. Freeland, E. Johnston-Halperin, D. D. Awschalom, and J. Shi, Phys. Rev. Lett. **91**, 187203 (2003).
[15] K. W. Edmonds, N. R. S. Farley, T. K. Johal, G. van der Laan, R. P. Campion, B. L. Gallegher, and C. T. Foxon, Phys. Rev. B **71**, 064418 (2005).
[16] D. J. Keavney, S. H. Cheung, S. T. King, M. Weinert, and L. Li, Phys. Rev. Lett. **95**, 257201 (2005).
[17] Y. Takeda, M. Kobayashi, T. Okane, T. Ohkochi, J. Okamoto, Y. Saitoh, K. Kobayashi, H. Yamagami, A. Fujimori, A. Tanaka, J. Okabayashi, M. Oshima, S. Ohya, P. N. Hai, and M. Tanaka, Phys. Rev. Lett. **100**, 247202 (2008).
[18] Y. K. Wakabayashi, S. Sakamoto, Y.-h. Takeda, K. Ishigami, Y. Takahashi, Y. Saitoh, H. Yamagami, A. Fujimori, M. Tanaka, and S. Ohya, Sci. Rep. **6**, 23295 (2016).
[19] R. Nakajima, J. Stohr, and Y. U. Idzerda, Phys. Rev. B **59**, 6421 (1999).
[20] See Supplemental Material at http://link.aps.org/supplemental/10.1103/PhysRevB.95.014417 for the sample preparation, crystallographic analyses, XAS and XMCD spectra of the $Ge_{0.91}Mn_{0.09}$ film, derivation of the FM and PM components of the XMCD-*H* curves, XMCD-*H* curves of the $Ge_{0.91}Mn_{0.09}$ film, Curie plots of the PM component of the XMCD intensity, derivation of the XAS spectra of the FM and PM components, and magnetization curves measured by SQUID.
[21] N. Sircar, S. Ahlers, C. Majer, G. Abstreiter, and D. Bougeard, Phys. Rev. B **83**, 125306 (2011).
[22] A. Jain, M. Jamet, A. Barski, T. Devillers, I.-S. Yu, C. Porret, P. Bayle-Guillemaud, V. Favre-Nicolin, S. Gambarelli, V. Maurel, G. Desfonds, J. F. Jacquot, and S. Tardif, J. Appl. Phys. **109**, 013911 (2011).
[23] P. Gambardella, L. Claude, S. Rusponi, K. J. Franke, H. Brune, J. Raabe, F. Nolting, P. Bencok, A. T. Hanbicki, B. T. Jonker, C. Grazioli, M. Veronese, and C. Carbone, Phys. Rev. B **75**, 125211 (2007).
[24] Y. Saitoh, Y. Fukuda, Y. Takeda, H. Yamagami, S. Takahashi, Y. Asano, T. Hara, K. Shirasawa, M. Takeuchi, T. Tanaka, and H. Kitamura, J. Synchrotron Radiat. **19**, 388 (2012).
[25] S. Picozzi, L. Ottaviano, M. Passacantando, G. Profeta, A. Continenza, F. Priolo, M. Kim, and A. J. Freema, Appl. Phys. Lett. **86**, 062501 (2005).
[26] G. van der Laan and B. T. Thole, Phys. Rev. B **43**, 13401 (1991).
[27] C. Hirai, H. Sato, A. Kimura, K. Yaji, K. Iori, M. Taniguchi, K. Hiraoka, T. Muro, and A. Tanaka, Phys. B **351**, 341 (2004).
[28] A. Stroppa, S. Picozzi, A. Continenza, and A. J. Freeman, Phys. Rev. B **68**, 155203 (2003).
[29] S. Yada, R. Okazaki, S. Ohya, and M. Tanaka, Appl. Phys. Exp. **3**, 123002 (2010).
[30] A. Kaminski and S. Das Sarma, Phys. Rev. Lett. **88**, 247202 (2002).
[31] M. Csontos, T. Wojtowicz, X. Liu, M. Dobrowolska, B. Janko, J. K. Furdyna, and G. Mihaly, Phys. Rev. Lett. **95**, 227203 (2005).